

Supplementary Information

Improving the hydrothermal stability of Al-rich Cu-SSZ-13 zeolite via Pr-ions modification

Mengyang Chen,^{‡a} Wenru Zhao,^{‡c} Yingzhen Wei,^b Shi-Bin Ren,^a Yuxiang Chen,^a Donghai Mei,^{*c} De-Man Han^{*a} and Jihong Yu^{*bd}

^a*School of Pharmaceutical and Chemical Engineering, Taizhou University, Taizhou 318000, P. R. China*

^b*State Key Laboratory of Inorganic Synthesis and Preparative Chemistry, College of Chemistry, Jilin University, Changchun, 130012, P. R. China.*

^c*School of Materials Science and Engineering, Tiangong University, Tianjin 300387, China.*

^d*International Center of Future Science, Jilin University, Changchun, 130012, P. R. China.*

[‡] These authors contributed equally.

^{*} Corresponding author

E-mail address: dhmei@tiangong.edu.cn; hdmtzc@126.com; jihong@jlu.edu.cn

Materials

Aluminum hydroxide ($\text{Al}(\text{OH})_3$, 76.5 wt%, Alfa Aesar), Ludox® HS-40 colloidal silica (40 wt%, Sigma-Aldrich), copper (II) acetate monohydrate ($\text{Cu}(\text{CH}_3\text{COO})_2 \cdot \text{H}_2\text{O}$, 98 wt.%, Beijing Innochem Chemical Reagent Co., Ltd), praseodymium(III) nitrate hexahydrate ($\text{Pr}(\text{NO}_3)_3 \cdot 6\text{H}_2\text{O}$, 99.99 wt%, Beijing Innochem Chemical Reagent Co., Ltd), sodium hydroxide (NaOH, 98 wt%, Beijing Chemical Works,) and N,N,N,-trimethyl-1-adamantane ammonium hydroxide (TMAdaOH, 25 wt%, Beijing Innochem Chemical Reagent Co., Ltd).

Synthesis of SSZ-13 zeolite

SSZ-13 zeolite was synthesized via a hydrothermal method. Typically, 0.2 g NaOH and 3 g TMAdaOH were dissolved in 7.15 g deionized water. Thereafter, 0.125 g $\text{Al}(\text{OH})_3$ was added under stirring. Afterwards, 1.4 g silica sol was added to the mixture under stirring. The molar ratio of the final mixture was 0.625 Al_2O_3 : 9 SiO_2 : 5 NaOH: 3.57 TMAdaOH: 522 H_2O . The mixture was transferred into a 20 mL autoclave and the hydrothermal synthesis was then carried out at 160 °C under static condition for 4 days. The obtained sample was centrifuged and washed several times with deionized (DI) water, then dried overnight at 80 °C, followed by calcination at 600 °C for 8 h.

Synthesis of CuPr-SSZ-13 zeolites

The SSZ-13 zeolite was ion-exchanged twice with 1 M NH_4NO_3 at 80 °C for getting NH_4 -SSZ-13. Then, NH_4 -SSZ-13 was exchanged with 0.004 M $\text{Cu}(\text{CH}_3\text{COO})_2$ at 80 °C for 1 h to get Cu-SSZ-13. Subsequently, 1 g Cu-SSZ-13 was mixed with a certain amount of praseodymium nitrate (0.018 g, 0.036 g and 0.072 g, respectively) and the mixture was uniformly ground. The final mixtures were calcined in a muffle oven at 750 °C for 4 h to get different CuPr-SSZ-13 zeolites via solid-state ion-exchanged method. The catalysts without or with Pr loadings were denoted as Cu-SSZ-13, $\text{CuPr}_{0.6}$ -SSZ-13-1, $\text{CuPr}_{1.2}$ -SSZ-13-2, $\text{CuPr}_{2.4}$ -SSZ-13-3, respectively. The 0.6, 1.2 and 2,4 stand for the content of Pr ions measured by ICP. The catalysts were hydrothermally aged in flowing air containing 10 vol.% H_2O at 800 °C for 10 h and denoted as Cu-SSZ-13-HTA, $\text{CuPr}_{0.6}$ -SSZ-13-1-HTA, $\text{CuPr}_{1.2}$ -SSZ-13-2-HTA, $\text{CuPr}_{2.4}$ -SSZ-13-3-HTA, respectively.

NH_3 -SCR catalytic test

SCR activity measurements of the catalysts were performed in a fixed-bed quartz reactor with an inner diameter of 6 mm. The catalyst of 0.1 g with particle size of 40–60 mesh was placed in the tubular reactor. The reaction conditions were as follows: 500 ppm

NO, 500 ppm NH₃, 5% O₂, 5% H₂O, N₂ as balance gas. The total flow rate was 500 mL/min and thus a normal gaseous hourly space velocity (GHSV) of ~ 200,000 h⁻¹. The inlet and outlet gas compositions were monitored by a FTIR spectrometer (MKS, MultiGas 2030HS). The NO conversion over the catalyst was calculated based on the inlet and outlet NO concentrations as follows:

$$\text{NO conversion (\%)} = \frac{\text{NO}_{\text{inlet}} - \text{NO}_{\text{outlet}}}{\text{NO}_{\text{inlet}}} \times 100(\%)$$

Characterization

The crystallinity and phase purity of the samples were characterized by power X-ray diffraction (XRD) on a D8 Advance diffractometer using Cu K_α radiation (λ = 1.5418 Å). XRD patterns for Rietveld refinement were performed on a Rigaku SmartLab X-ray diffractometer equipped with a PhotonMax high-flux 9 kW rotating anode X-ray source (CuK_{α1} target, λ = 1.5406 Å) and a D/teX Ultra 250 silicon strip detector using transmission diffraction geometry. Scanning electron microscopy (SEM) images were measured with JEOL S-4800. Transmission electron microscopy (TEM) images and elemental mapping images were recorded on a Thermo Scientific Talos F200i. Chemical compositions were determined with inductively coupled plasma (ICP) analyses (Thermo Fisher Scientific iCAP7600 DUO). Nitrogen adsorption/desorption measurements were carried out on a Micromeritics ASAP 2020 HD88 at 77.35 K after the samples were degassed at 350 °C under vacuum. The temperature-programmed desorption of ammonia (NH₃-TPD) experiments were performed using a Micromeritics AutoChemII 2920 automated chemisorption analysis unit with a thermal conductivity detector (TCD) under helium flow. The electron paramagnetic resonance (EPR) signals of Cu²⁺ species were recorded at 150 K on an EMXPLUS10/12 ESR spectrometer (Bruker Company, Karlsruhe, Germany) in the region of 2200–3800 G. Solid-state ²⁷Al MAS NMR experiments were performed on Bruker Avance Neo 600Mz WB spectrometer with BBO MAS probe operating at a magnetic field strength of 14.1 T. The H₂-TPR experiments were performed on an AutoChemII 2920 analyzer. The sample was pretreated in air atmosphere at 500 °C for 1 h before TPR was conducted in 10% H₂/Ar at a flow rate of 50 ml/min. X-ray photoelectron spectroscopy (XPS) spectra were measured using a Thermo ESCALAB 250 spectrometer with monochromatized Al K_α excitation. Ultraviolet–Visible diffuse reflection spectrums (UV–vis DRS) were obtained in the range of 200–800 nm on a U-4100 at the ambient temperature.

DFT calculations

All periodic density functional theory (DFT) calculations were performed with mixed Gaussian and plane wave basis sets implemented in the CP2K code.¹ The core electron was represented by norm-conserving Goedecker-Teter-Hutter pseudopotentials,²⁻⁴ and the valence electron wavefunctions were expanded in a triple-zeta basis set with polarization functions⁵ along with an auxiliary plane wave basis set with an energy cutoff of 400 Ry. The generalized gradient approximation exchange-correlation functional of Perdew, Burke, and Enzerhof (PBE) was used.⁶ Test calculations showed that the total energy change of the system was negligible (<0.01 eV) when the maximum force convergence criteria of 0.001 Hartree/Bohr was used. Each reaction intermediate structure was optimized with the Broyden-Fletcher-Goldfarb-Shanno (BGFS) algorithm with the SCF convergence criteria of 1.0×10^{-8} a.u. To account for the long-range van der Waals (vdW) interactions, the DFT-D3 scheme with an empirical damped potential term was added to the electronic energy.⁷ The climbing image elastic band (CI-NEB) method^{8,9} was used to determine the transition states of elementary reaction steps in the formation of Cu(OH)₂ over Cu-SSZ-13 and Cu-Pr-SSZ-13 zeolites. Each transition state was located with five intermediate images along the reaction pathway between the initial and final states. Each identified transition state was further confirmed by the vibrational frequency analysis, in which only one imaginary frequency was found at the transition state.¹⁰

The Gibbs free energy including zero-point energy (ZPE), internal energy, and entropy along the reaction pathway was calculated using the standard statistical mechanics method,¹¹⁻¹³ i.e.,

$$G = E_{\text{elec}} + E_{\text{ZPE}} + U - TS$$

where E_{elec} is the electronic term, E_{ZPE} is the ZPE contribution, U is the internal energy, S is the entropy, and T (1023 K, typical experimental condition) is the temperature. The electronic term (E_{elec}) is directly calculated from DFT calculations. The ZPE contribution is given by

$$\text{ZPE} = \sum_i \frac{h\nu_i}{2}$$

Where h and ν_i are Planck's constant and vibrational frequencies. The vibrational frequencies are calculated in the framework of the localized harmonic oscillator approximation with a displacement of 0.01 Å. In the vibrational frequency calculation, only mobile reactants/intermediates were considered while other atoms on the SSZ-13 framework were fixed. Since spurious imaginary and low-lying vibrational frequencies ($< 50 \text{ cm}^{-1}$) were usually obtained in the vibrational analysis owing to the presence of frustrated translational and rotational of the reactant species in the zeolite pores. As suggested by previous studies,^{13,14} a normal mode of 50 cm^{-1} was adopted to replace all the imaginary and low-lying vibrational frequencies obtained from vibrational calculations. Similarly, the Gibbs free energy of activation ΔG^\ddagger was calculated as follows:

$$\Delta G^\ddagger = (E_{elec}^{TS} - E_{elec}^{IS}) + \Delta E_{ZPE}^\ddagger + \Delta U^\ddagger - T\Delta S^\ddagger$$

where E_{elec}^{TS} and E_{elec}^{IS} are the electronic energy difference between the transition state (TS) and the initial state (IS) of elementary reaction step, respectively. Correspondingly, ΔE_{ZPE}^\ddagger , ΔU^\ddagger , ΔS^\ddagger are the ZPE energy, internal energy and entropy difference between the TS and the IS states.

The SSZ-13 zeolite structure was modelled using 2 hexagonal unit cells (72 T atoms in total) with the size parameters of $13.6750 \times 23.6858 \times 14.7670 \text{ \AA}^3$. A total of 10 Si atoms within the SSZ-13 model structure were replaced by 10 Al atoms, and 10 H atoms were then introduced at the O₁ position of four O atoms connected with the Al atom to keeping the structure charge neutral.¹⁵⁻¹⁷ As such, the constructed H-SSZ-13 zeolite model has a chemical formula of Al₁₀H₁₀Si₆₂O₁₄₄ with a Si/Al ratio of 6.2, which is consistent to the experimental Si/Al ratio for the actual Cu-SSZ-13 catalysts used in this study. On the basis of Cu and Pr weight fraction (wt%) in Cu-Pr-SSZ-13 zeolites, two Cu and one Pr atoms in the form of Z₂Cu²⁺, [ZCu²⁺(OH)]⁺, [Z₂Pr³⁺(OH)]²⁺ and [ZPr³⁺(OH)₂]⁺ were introduced into the H-SSZ-13 zeolite. The Z₂Cu²⁺/[ZCu²⁺(OH)]⁺ located in the window of 6-membered ring (6MR) balanced with 2/1 framework negative charges (removing two/one original H⁺) were optimized as the initial configurations. The [ZPr³⁺(OH)₂]⁺ located in the window of 8-membered ring (8MR) and the CHA cage balanced with 1 framework negative charges (removing one original H⁺) while the [Z₂Pr³⁺(OH)]²⁺ located in the window of 8-membered ring (8MR) and the CHA cage balanced with 2 framework negative charges (removing two original H⁺) were optimized as the initial configurations.

Figures and Tables

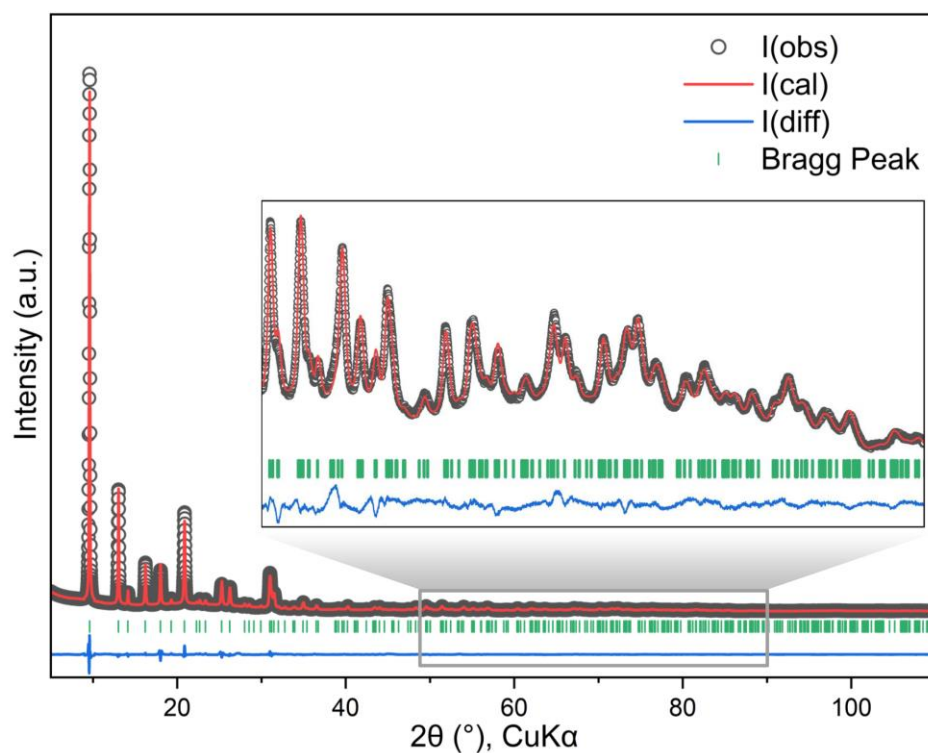


Fig. S1 Crystallographic structure of Pr-SSZ-13 with 1.2 wt% Pr loading and its corresponding final Rietveld refinement plots. The observed, calculated, and difference curves are in black, red, and blue, respectively. The vertical bars indicate the positions of the Bragg peaks ($\lambda=1.5406 \text{ \AA}$).

GOF	R_p	R_{wp}
3.22	0.0288	0.0418

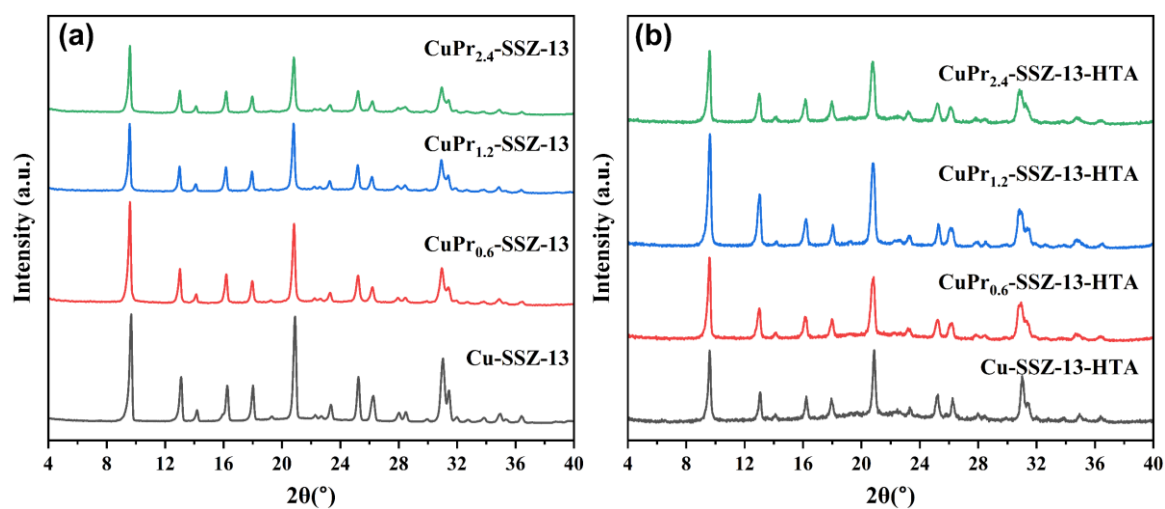


Fig. S2 The XRD patterns of fresh (a) and aged (b) SSZ-13 samples.

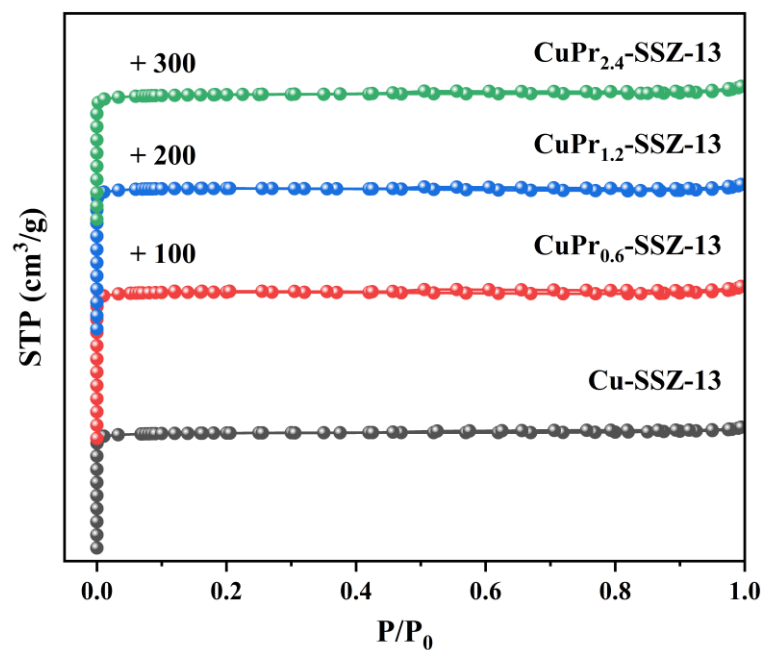


Fig. S3 Nitrogen adsorption-desorption isotherms of Cu-SSZ-13 and CuPr-SSZ-13 zeolites.

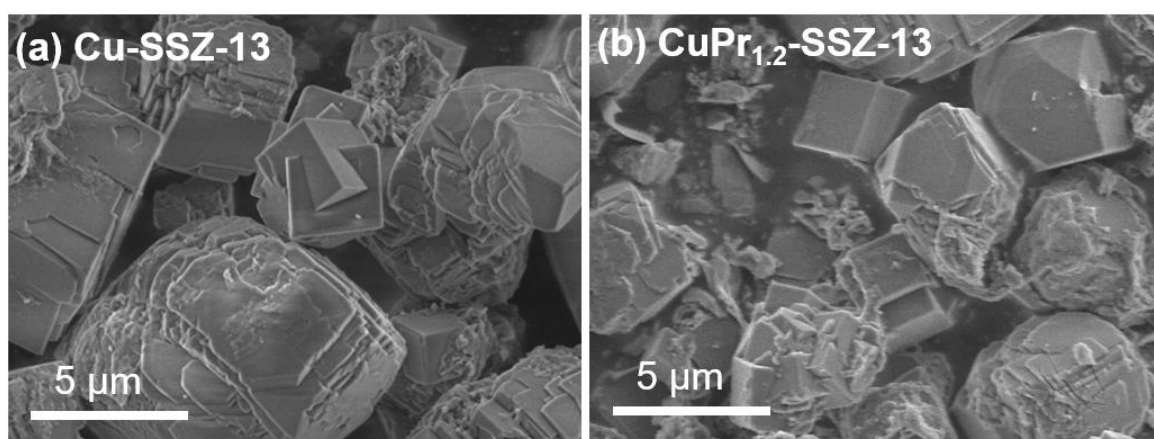


Fig. S4 The SEM images of (a) Cu-SSZ-13 and (b) CuPr_{1.2}-SSZ-13.

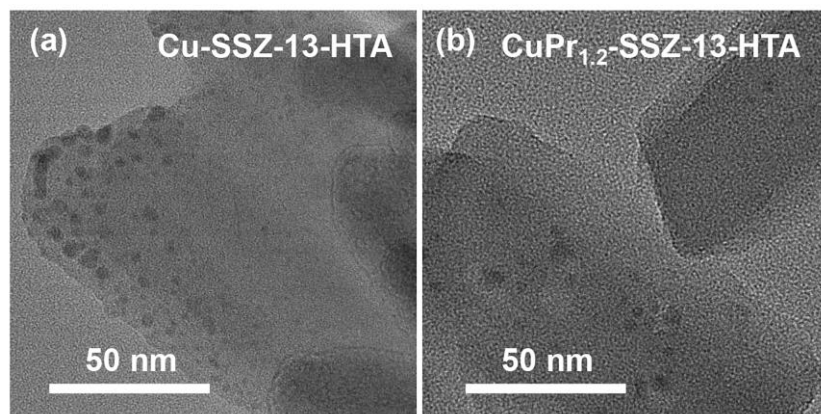


Fig. S5 TEM images of (a) Cu-SSZ-13, (b) CuPr_{1.2}-SSZ-13, (c) Cu-SSZ-13-HTA and (d) CuPr_{1.2}-SSZ-13-HTA.

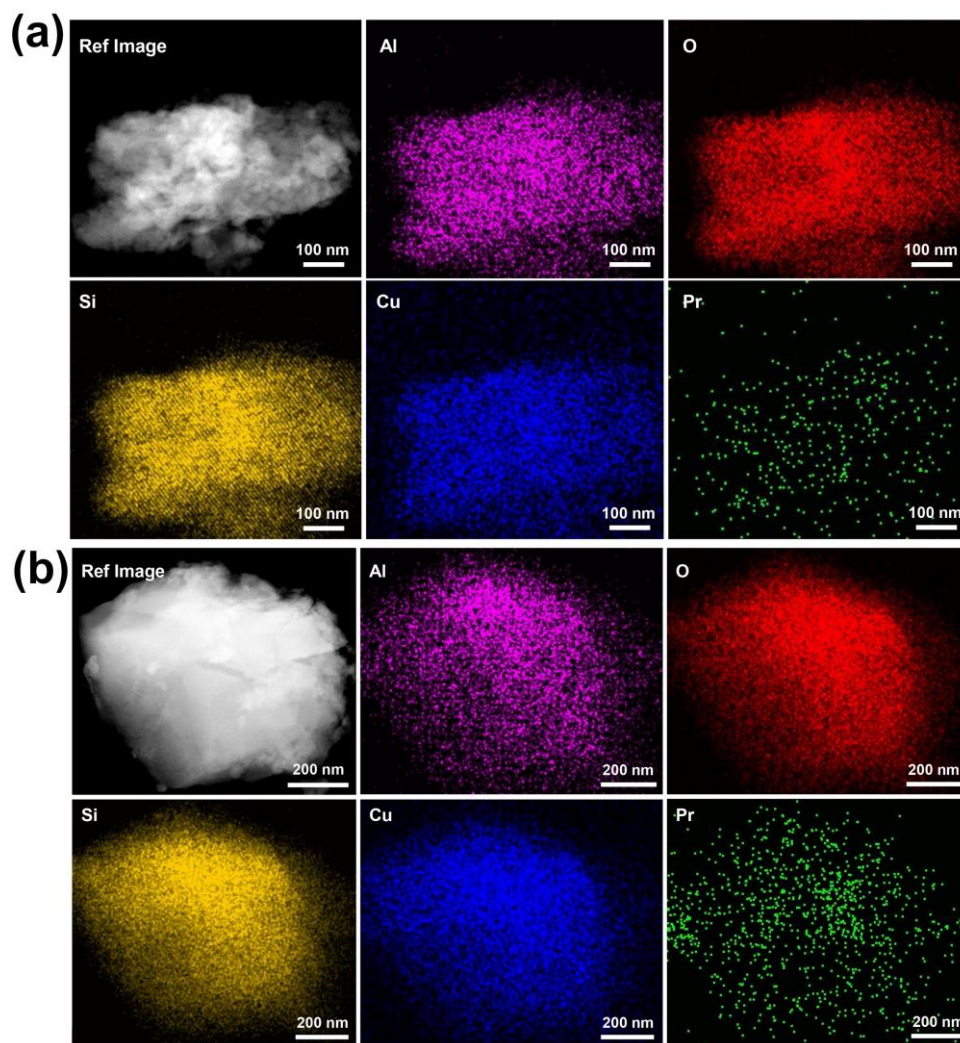


Fig. S6 Elemental mapping images of (a) CuPr_{1.2}-SSZ-13 and (b) CuPr_{1.2}-SSZ-13-HTA.

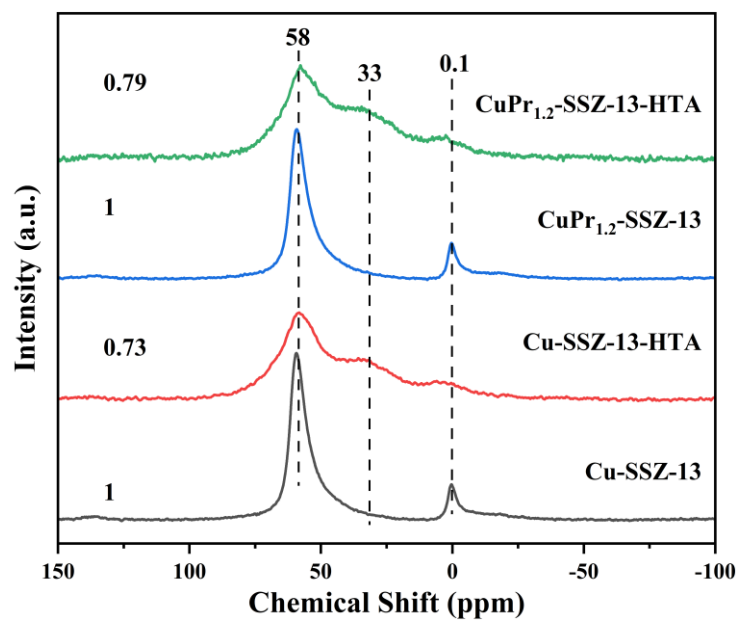


Fig. S7 ^{27}Al MAS NMR spectra of Cu-SSZ-13 and $\text{CuPr}_{1.2}$ -SSZ-13 before and after hydrothermal aging.

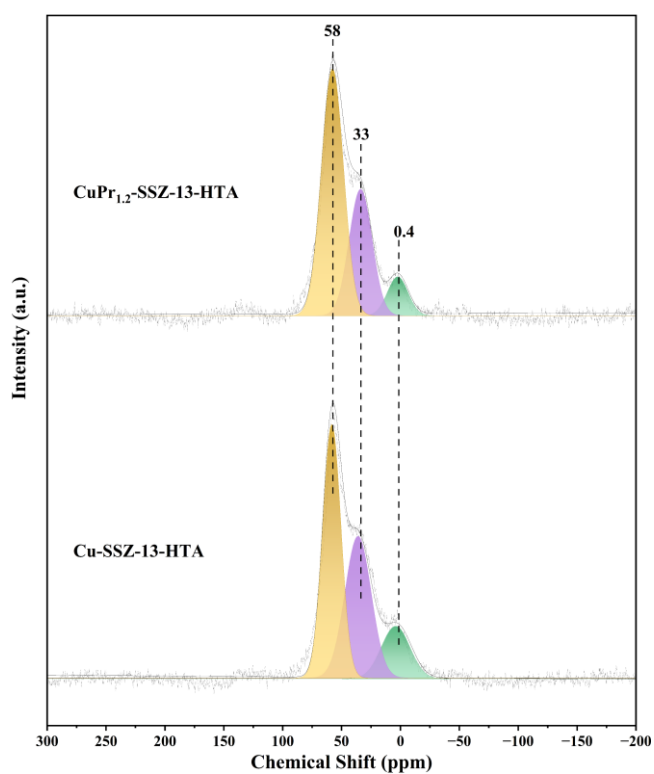


Fig. S8 The distributions of Al for Cu-SSZ-13-HTA and $\text{CuPr}_{1.2}$ -SSZ-13-HTA.

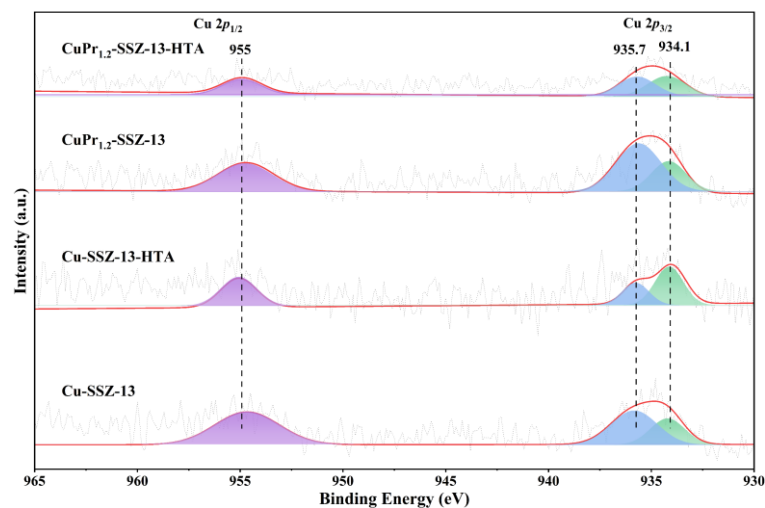


Fig. S9 Cu 2p XPS spectra of Cu-SSZ-13, Cu-SSZ-13-HTA, CuPr_{1.2}-SSZ-13 and CuPr_{1.2}-SSZ-13-HTA.

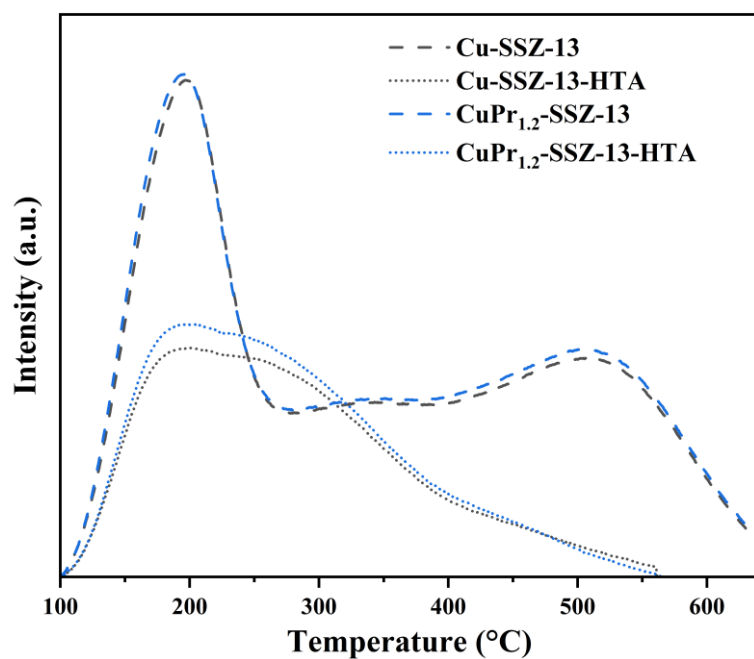


Fig. S10 NH₃-TPD profiles of Cu-SSZ-13, Cu-SSZ-13-HTA, CuPr_{1.2}-SSZ-13 and CuPr_{1.2}-SSZ-13-HTA.

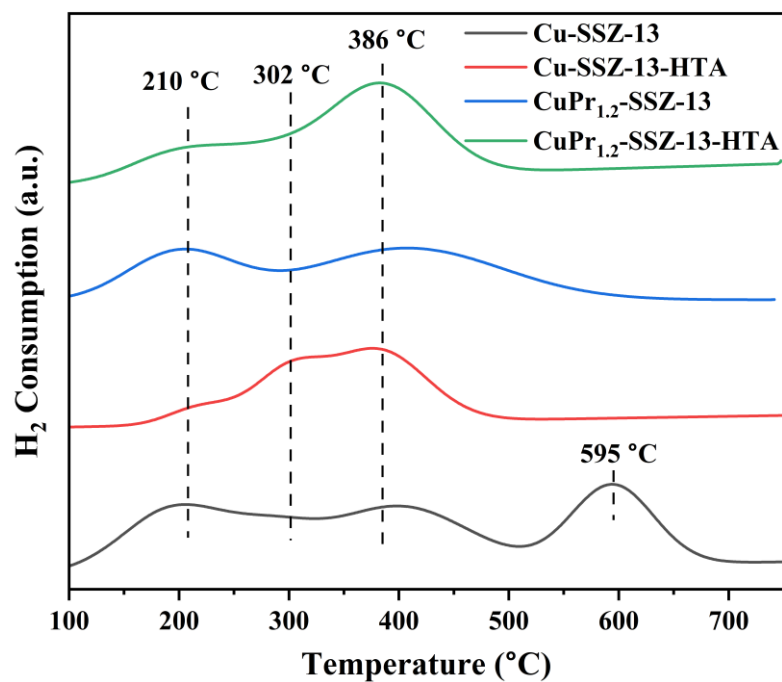


Fig. S11 H₂-TPR profiles of Cu-SSZ-13, Cu-SSZ-13-HTA, CuPr_{1.2}-SSZ-13 and CuPr_{1.2}-SSZ-13-HTA.

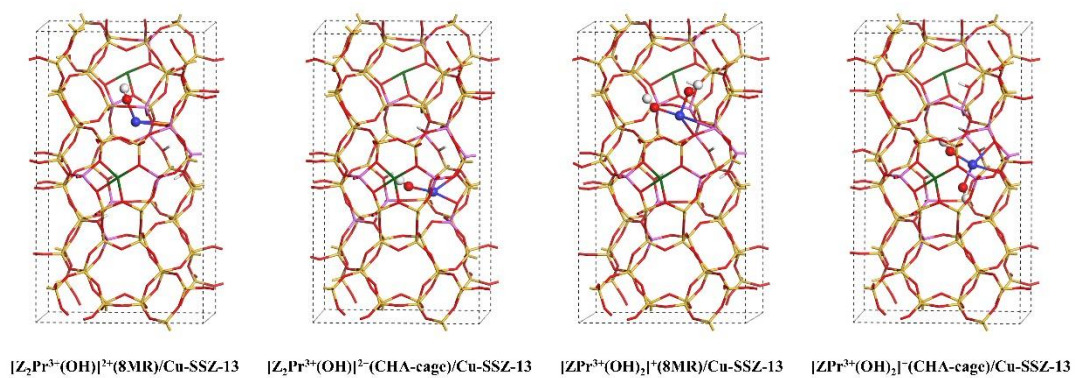


Fig. S12 The optimized structures of Pr ion in the Cu-SSZ-13 zeolite. The Si, O, Al, Cu, H, and Pr atoms are colored in yellow, red, magenta, blue, white and green, respectively.

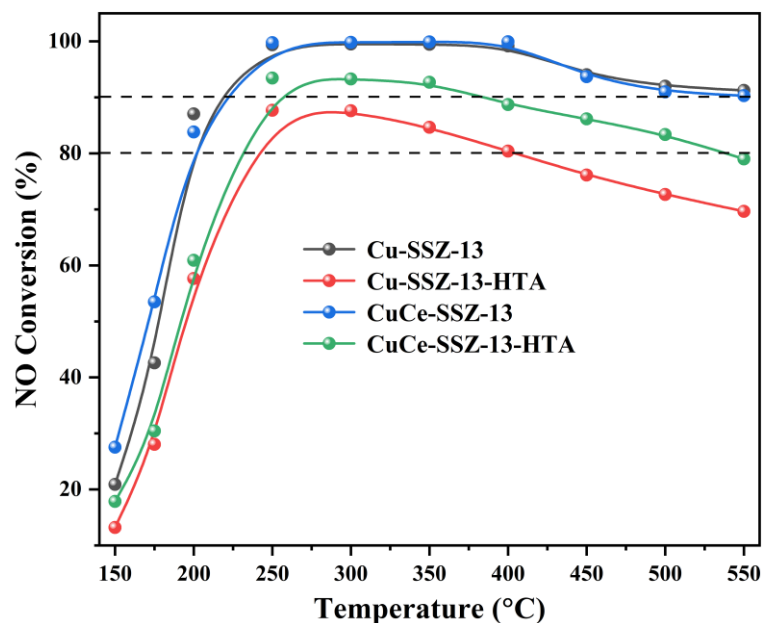


Fig. S13 NO conversion as a function of temperature for Cu-SSZ-13 and CuCe-SSZ-13 samples before and after hydrothermal aging.

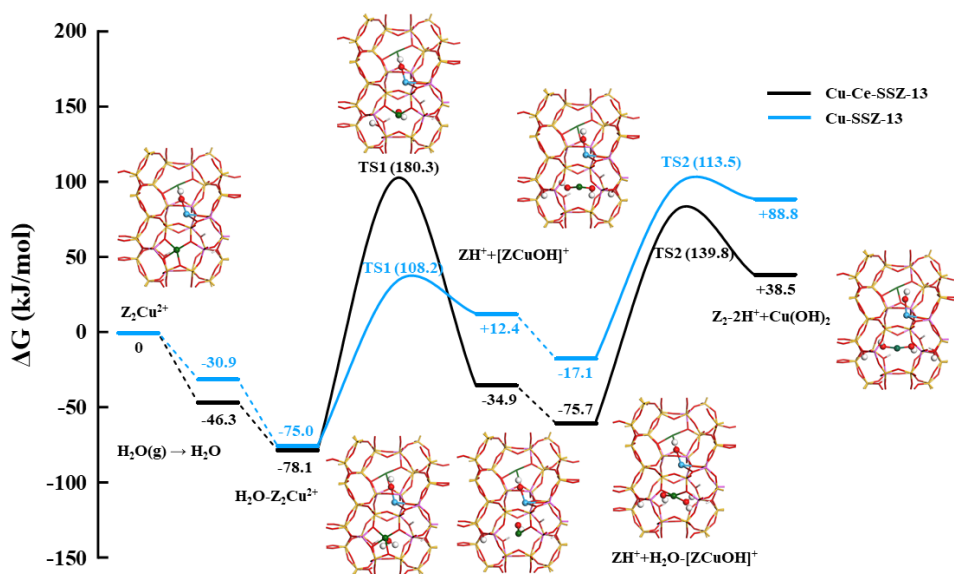


Fig. S14 DFT calculated free energy profiles for the transformation of Z_2Cu^{2+} ion at the 6MR in the absence/presence of $[ZCe^{3+}(OH)_2]^+$ at the 8MR under the hydrothermal condition ($T=1023$ K). The Si, O, Al, Cu, H, and Ce atoms are colored in yellow, red, magenta, blue, white and green, respectively.

Tables

Table S1. Refined atomic positions obtained from Rietveld refinement of Pr-SSZ-13 with 1.2 wt% Sm loading. Water molecules are omitted in this list.

Atom	x	y	z	Occ
Si1	0.43865	0.33333	0.43699	0.875
Al1	0.43865	0.33333	0.43699	0.125
O1	0.3571	0.3571	0.5	1.000
O2	0.4043	0.33333	0.33333	1.000
O3	0.57034	0.42966	0.4529	1.000
O4	0.4269	0.21347	0.4674	1.000
Pr1	0.672	0.836	0.361	0.009
Pr2	0.66667	0.33333	0.33333	0.010

Table S2. Chemical composition and texture property of SSZ-13 zeolites.

Sample	Si/Al ^a	Cu wt% ^a	Pr wt% ^a	S _{BET} (m ² /g) ^b	V _{micro} (cm ³ /g) ^c
Cu-SSZ-13	6.24	2.28	/	512	0.24
CuPr _{0.6} -SSZ-13	6.23	2.30	0.6	467	0.22
CuPr _{1.2} -SSZ-13	6.15	2.29	1.2	446	0.21
CuPr _{2.4} -SSZ-13	6.16	2.30	2.4	409	0.19
Pr-SSZ-13	6.18	/	/	/	/

^a Determined by ICP, ^b S_{BET} (total surface area) calculated by applying the BET equation, ^c V_{micro} (micropore area) calculated using the t-plot method.

Table S3. The content of different Al distributions for Cu-SSZ-13-HTA and CuPr_{1.2}-SSZ-13-HTA.

Sample	Tetraordinated Al	Pentacoordinated Al	Hexacoordinated Al
Cu-SSZ-13-HTA	52.9%	31.8%	15.3%
CuPr _{1.2} -SSZ-13-HTA	60.4%	28.1%	11.5%

References

1. J. VandeVondele, M. Krack, F. Mohamed, M. Parrinello, T. Chassaing and J. Hutter, *Comput. Phys. Commun.*, 2005, **167**, 103-128.
2. S. Goedecker, M. Teter and J. Hutter, *Phys. Rev. B: Condens. Matter.*, 1996, **54**, 1703-1710.
3. M. Krack and M. Parrinello, *Phys. Chem. Chem. Phys.*, 2000, **2**, 2105-2112.
4. C. Hartwigsen, S. Goedecker and J. Hutter, *Phys. Rev. B*, 1998, **58**, 3641-3662.
5. J. VandeVondele and J. Hutter, *J. Chem. Phys.*, 2007, **127**, 114105.
6. J. P. Perdew, K. Burke and M. Ernzerhof, *Phys. Rev. Lett.*, 1996, **77**, 3865-3868.
7. S. Grimme, J. Antony, S. Ehrlich and H. Krieg, *J. Chem. Phys.*, 2010, **132**, 154104.
8. G. Henkelman, B. P. Uberuaga and H. Jónsson, *J. Chem. Phys.*, 2000, **113**, 9901-9904.
9. G. J. H. Mills and G. K. Schenter, *Surf. Sci.*, 1994, **324**, 305-337.
10. R. Grybos, L. Benco, T. Bucko and J. Hafner, *J. Chem. Phys.*, 2009, **130**, 104503.
11. M. John, K. Alexopoulos, M.-F. Reyniers and G. B. Marin, *J. Catal.*, 2015, **330**, 28-45.
12. F. Gao, D. Mei, Y. Wang, J. Szanyi and C. H. Peden, *J. Am. Chem. Soc.*, 2017, **139**, 4935-4942.
13. D. Mei and J. A. Lercher, *AIChE J.* 2017, **63**, 172-184.
14. M. John, K. Alexopoulos, M.-F. Reyniers and G. B. Marin, *ACS Catal.*, 2016, **6**, 4081-4094.
15. W. Xue and D. Mei, *Chem. Eng. J.*, 2022, **444**, 136671.
16. M. Chen, J. Li, W. Xue, S. Wang, J. Han, Y. Wei, D. Mei, Y. Li and J. Yu, *J. Am. Chem. Soc.*, 2022, **144**, 12816-12824.
17. Y. Cui, Y. Wang, D. Mei, E. D. Walter, N. M. Washton, J. D. Holladay, Y. Wang, J. Szanyi, C. H. F. Peden and F. Gao, *J. Catal.*, 2019, **378**, 363-375.